Mechanism of Mg^{2+}-accompanied product release in sugar nucleotidyltransferases

Neha Vithani[1$], Pravin Kumar Ankush Jagtap[1,4$], Sunil Kumar Verma[1,5$], Ravi Tripathi[3,6], Shalini Awasthi[3], Nisanth N. Nair[3*] and Balaji Prakash[2,7*]

[1]Department of Biological Sciences and Bioengineering, Indian Institute of Technology, Kanpur 208016, India
[2]Department of Molecular Nutrition, CSIR-Central Food Technological Research Institute, Mysore, 570020, India
[3]Department of Chemistry, Indian Institute of Technology, Kanpur 208016, India
[4]Present address: EMBL, Heidelberg, 69117, Germany
[5]Present address: University of Texas Medical Branch, Galveston, United States
[6]Present address: Ruhr-University, Bochum, Germany
[7]Lead contact

*Authors for correspondence
Email: balaji.prakash@cftri.res.in, nnair@iitk.ac.in
[$]These authors contributed equally.

Summary: The nucleotidyltransfer reaction, catalyzed by sugar nucleotidyltransferases (SNTs), is assisted by two active site Mg^{2+} ions. While studying this reaction using X-ray crystallography, we captured snapshots of the pyrophosphate (product) as it exits along a pocket. Surprisingly, one of the active site Mg^{2+} ions remains coordinated to the exiting pyrophosphate. This hints at the participation of Mg^{2+} in the process of product release, besides its role in catalyzing nucleotidyltransfer. These observations are further supported by enhanced sampling molecular dynamics simulations. Free energy computations suggest that the product release is likely to be rate limiting in SNTs, and the origin of the high free energy barrier for product release could be traced back to the "slow" conformational change of an Arg residue at the exit end of the pocket. These results establish a dual role for Mg^{2+}, and propose a general mechanism of product release during the nucleotidyltransfer by SNTs.

Introduction

Sugar nucleotidyltransferases (SNTs) catalyze nucleotidyltransfer reaction and produce a sugar-nucleotide and pyrophosphate (POP). Sugar-nucleotides participate in diverse biological processes such as cell growth, antigen synthesis, synthesis of cell-wall components in prokaryotes and plants, and sugar metabolism in eukaryotes (Frey, 1996; McNeil et al., 1990; Chang et al., 1996). GlmU is a member of SNT family. GlmU synthesizes a sugar-nucleotide called UDP-GlcNAc using the substrates UTP and GlcNAc-1-P (N-acetylglucosamine-1-phosphate) (Barreteau et al., 2008; Mengin-Lecreulx et al., 1982). Like all other SNTs, GlmU requires Mg^{2+} ions for its nucleotidyltransfer reaction (Mengin-Lecreulx and van Heijenoort, 1994).

In our previous work, we determined a structure of GlmU bound to two Mg^{2+} ions (Mg^{2+}_A and Mg^{2+}_B) and the products UDP-GlcNAc (termed here as UD1) and POP (Jagtap et al., 2013). This structure for the first time depicted two Mg^{2+} ions at the active site of GlmU, with the the simultaneous presence of both the products. In that study, it was inferred that GlmU employs two Mg^{2+} ions (termed Mg^{2+}_A and Mg^{2+}_B) for the catalysis (Jagtap et al., 2013). Mg^{2+}_A was coordinated to two active site residues, two water molecules and two phosphate oxygens of UD1. Mg^{2+}_B was coordinated to three water molecules, a phosphate oxygen of UD1 and two phosphate oxygens of POP (Supporting information; Fig. S1b). It was proposed that Mg^{2+}_A stabilizes the substrates for the reaction and Mg^{2+}_B would stabilize the transition state. A report on another SNT called Kdo cytidyltransferase (KdsB) also depicted similar roles for the Mg^{2+} ions (Schmidt et al., 2011). The two-metal-ion mechanism proposed for SNTs is termed 'Mechanism-B'. DNA/RNA polymerases that perform similar nucleotidyltransfer reaction on the growing nucleic acid chain also employ a two-metal-ion mechanism (termed 'Mechanism-A') (Sosunov et al., 2003; Steitz and Steitz, 1993). Besides, POP is formed as one of the products in SNTs as well as DNA/RNA polymerases. 'Mechanism-A' and 'Mechanism-B' differ in the way two Mg^{2+} ions (Mg^{2+}_A and Mg^{2+}_B) are stabilized at the active site (Supporting information; Fig. S1). An important distinction is that Mg^{2+}_B in 'Mechanism-A' makes one of its coordination interactions with an active site residue, while in 'Mechanism-B' it does not make any coordination interaction with the active site residues (Supporting information; Fig. S1). Despite these differences, the catalytic roles assigned to each Mg^{2+} ion remain the same (Lassila et al., 2011; Steitz and Steitz, 1993). Computational studies on RNA polymerases have shown that

POP is released as POP-Mg^{2+}_{B} complex (Da et al., 2012, 2013). In the crystal structure of GlmU and a related SNT, it was seen that Mg^{2+}_{B} does not make any coordination interaction with the active site residues (Jagtap et al., 2013; Schmidt et al., 2011). Instead, it makes coordination interactions with the products UD1 and POP, and with water molecules. Based on this observation, it was previously speculated that Mg^{2+}_{B} might accompany POP during its exit (Schmidt et al., 2011).

Here, we investigate POP release pathway in GlmU and the participation of Mg^{2+}_{B} in this process of product release, which is as important as product formation, as it could be a rate-determining step in enzymes where products are stabilized at the active site. In this work, we present three distinct structural snapshots of GlmU determined in complex with the products (UD1 and POP) and two Mg^{2+} ions. These structural snapshots capture POP in complex with Mg^{2+}_{B}, in two distinct positions inside a pocket lined by positively charged residues. This suggested that POP-Mg^{2+}_{B} complex would exit the active site through this pocket. To study the mechanism for POP release from the active site into the bulk solvent, we employed umbrella sampling (US) (Kästner, 2011; Torrie and Valleau, 1974) and temperature accelerated sliced sampling (TASS) (Awasthi and Nair, 2017) simulations. These simulations elucidate that POP is indeed released through the pocket, as POP-Mg^{2+}_{B} complex. During its exit, POP-Mg^{2+}_{B} passes through two intermediate states, which are stabilized by the residues lining the pocket. One of these intermediates is also captured in our crystallographic snapshots. Computational studies in RNA polymerases have similarly depicted the release of POP-Mg^{2+}_{B} complex, via a few intermediate states (Da et al., 2012, 2013).

A residue lining the pocket, Arg19, is identified to be critical for POP release into the bulk solvent. In the intermediate states, it provides stabilizing interactions to POP inside the pocket and subsequently, it flips the side chain conformation, which brings POP-Mg^{2+}_{B} out of the pocket. Arg19 and other residues lining the pocket are highly conserved in SNTs and Mg^{2+}_{B} too, is commonly employed by all SNTs (Jagtap et al., 2013). Therefore, the exit pathway and mechanism for POP release proposed in this study is likely to be conserved in other SNTs as well.

Results and Discussion

Structural snapshots depicting pyrophosphate release in complex with a Mg^{2+} ion

We have previously determined a crystal structure of GlmU bound to the products (UD1 and POP) and two Mg^{2+} ions (Mg^{2+}_A and Mg^{2+}_B) (Jagtap et al., 2013). This structure (PDB ID: 4G87) with both the products bound at the active site, following the uridyltransfer reaction, is termed GlmU[S1]. Here, S1 implies 'snapshot 1'. GlmU[S1] was obtained by soaking GlmU[Apo] crystals with the substrates GlcNAc-1-P and UTP. In GlmU[S1], Mg^{2+}_B has an octahedral hexa-coordination geometry. Mg^{2+}_B is coordinated to an oxygen of PA phosphate of UD1, two oxygen atoms of POP and three water molecules (Supporting information; Fig. S1b). Unlike Mg^{2+}_A, Mg^{2+}_B does not make any coordination interaction with the active site amino acids. This has also been observed in the crystal structure of another sugar nucleotidyltransferase KdsB, based on which it was speculated that Mg^{2+}_B would exit together with POP (Schmidt et al., 2011).

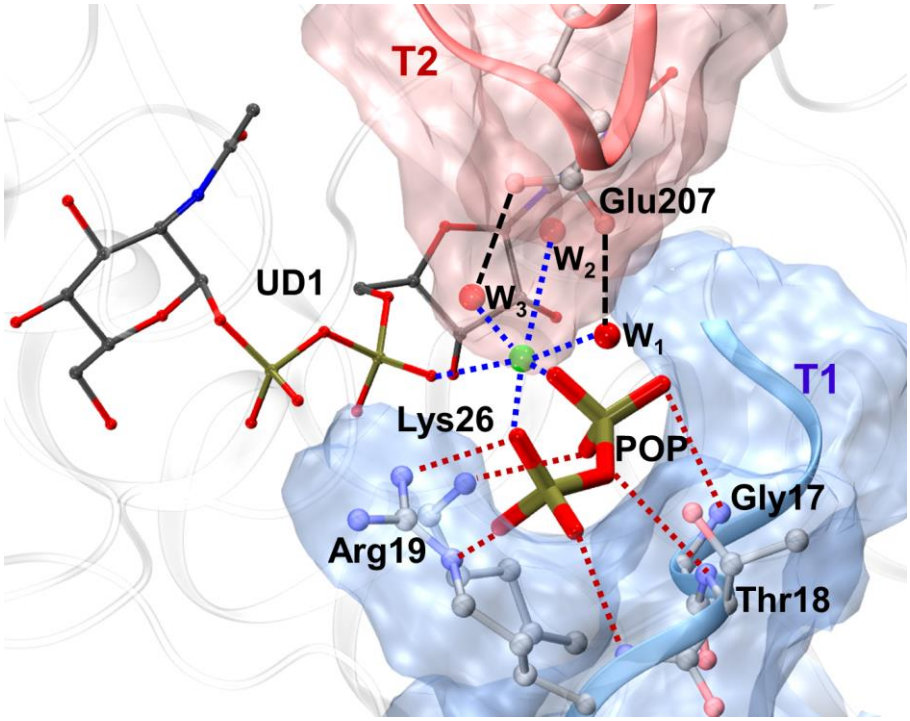

Figure 1. Pocket-like structure (front view), enclosed by T1 and T2 regions, in the snapshot GlmU[S1]. T1 and T2 regions are shown by blue and red colored ribbons, respectively, together with their surface representation. POP (shown in stick representation) is occupied in the pocket. Interactions of POP (red colored dotted line) and Mg^{2+}_B (blue colored dotted line) are depicted. The interacting residues, UD1 and water molecules (W_1, W_2 and W_3) are shown in ball and stick representation (without the hydrogen atoms for clarity). Color code: gray (carbon), red (oxygen), blue (nitrogen) and green (Mg^{2+}_B).

Analyzing the structure GlmU[S1], we find that POP is snugly occupied in a pocket-like structure (Fig. 1). A part of this pocket is lined by positively charged amino acids (Arg19 and Ly26), which are also important for binding and stabilizing the substrate UTP (Jagtap et al., 2013). We term this region of the pocket as T1 region. T1 region is formed by the backbone amides and side chains of Gly17, Thr18, Arg19 and also the side chain of Lys26; all of these make H-bond interactions with POP (Fig. 1). Additionally, coordination interactions of Mg^{2+}_{B} with both the products (UD1 and POP), stabilize them together at the active site. Mg^{2+}_{B} also makes coordination interactions with three water molecules, of which two are stabilized by Glu207 side chain (Fig. 1). Glu207 is present in a loop that forms the upper part of the pocket. This region is termed T2. Thus, T1 and T2 regions together form the entire exit pocket and contribute stabilizing interactions for POP and Mg^{2+}_{B} (Fig. 1). The shape and charge complementarity between POP and the pocket suggested that free diffusion of the POP following product formation would be prohibited. We presumed this to be a likely reason for the retention of POP at the active site. Apart from GlmU[S1], serendipitously, we also obtain two different crystal structures depicting different positions for POP, when $GlmU^{Mtb}$[Apo] crystals were soaked in substrates GlcNAc-1-P and UTP. These two structures are termed GlmU[S2] and GlmU[S3]. A comparison of these suggests that they represent snapshots of the process of POP release, where POP was seen to occupy two distinct positions – position A and/or position B – in these (Fig. 1 & 2).

As detailed above, GlmU[S1] represents a structure where products UD1 and POP are retained at the active site, in a position immediately following their formation (Fig. 1). Interestingly, in the snapshot GlmU[S2], POP and Mg^{2+}_{B} were found in two distinct positions. POP found at position A is termed APOP, while POP found at position B is termed BPOP (Fig. 2a). In GlmU[S2], APOP and BPOP were modeled with occupancies of 0.5 for each (Supporting information; Fig. S2a). Corresponding to these, Mg^{2+}_{B} was similarly modeled in two distinct positions with occupancies 0.5 for each (Supporting information; Fig. S2a). APOP superposes well with POP seen in GlmU[S1], while BPOP is shifted by ~3 Å with respect to APOP (Fig. 2). In the snapshot GlmU[S3], POP and Mg^{2+}_{B} occupy a single position and they were modeled with an occupancy 1.0 (Supporting information; Fig. S2b). Although not identical, POP in GlmU[S3] overlaps well with BPOP seen in GlmU[S2] (Fig. 2b).

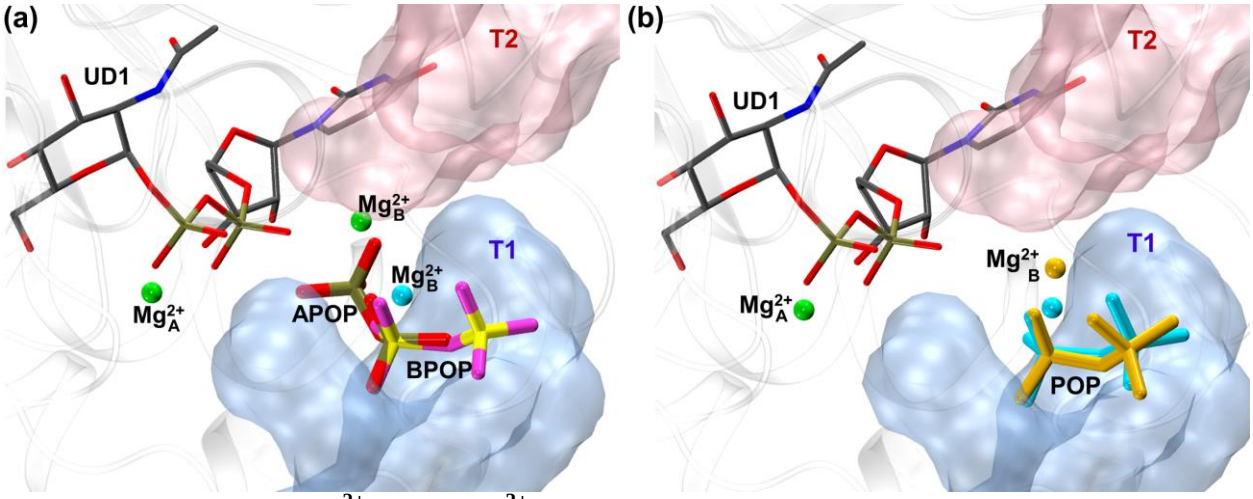

Figure 2. UD1, POP, Mg^{2+}_A, and Mg^{2+}_B bound at the active site in the snapshots GlmU[S2] and GlmU[S3]. (a) APOP and BPOP in GlmU[S2] are shown with their respective Mg^{2+}_B ions (shown as green and cyan colored spheres, respectively). **(b)** Structural overlap of BPOP of GlmU[S2] and GlmU[S3] (shown in cyan and yellow, respectively; Mg^{2+}_B ions are shown as spheres in the corresponding colors). Regions T1 (pink color) and T2 (blue color) are shown in surface representation.

Further, in similar soaking experiments with an extended soaking time or increased substrate concentration, we attempted to capture a state where POP has moved beyond the position B. However, in all the structures that we determined from such experiments, we found that POP only occupies position B and not beyond. This hinted at the inability of POP to completely exit the pocket. In the position B, POP is stabilized by T1 region through its interactions with backbone amides and the side chains of Gly17, Thr18 and Arg19. In this position, however, the interaction with Lys26 is conspicuously absent. One of the waters coordinating to Mg^{2+}_B is stabilized by Gln205 and Glu207 present in T2 loop. Thus, it appears T1 and T2 regions continue to provide stabilization to POP as it moves outwards.

It is intriguing that POP did not exit the active site in any of these snapshots. An analysis of the crystal contacts in these reveals that the path by which POP would exit the pocket is occluded by a surface patch of negative potential from a neighboring symmetry-related molecule in the crystal (Fig. S2c, S2d). This is likely to prevent negatively charged POP from leaving the pocket. Thus, in all the snapshots, POP moves only up to position B and does not completely exit the active site. In the absence of the occlusion by a symmetry-related molecule, as would be the case in solution, POP would have exited through the pocket into the solvent.

In order to study the mechanism of complete release of POP from the active site of GlmU into the solvent, we employed MD simulations combined with US and TASS(Awasthi and Nair, 2017) simulations. MD simulations were carried out using GlmU[S1] as the initial coordinates (PDB ID: 4G87), which represents the state where POP has just formed. We carried out equilibrium MD simulations for the solvated enzyme prior to performing US and TASS simulations (See 'STAR Methods' for further details). Root mean square deviation (RMSD) of the backbone atoms measured with respect to the original crystal structure (GlmU[S1]) is less than 1.6 Å during 5 ns NVT simulation. RMSD for active site residues Gly17, Thr18, Arg19, Lys26, Ala238 and Asn239 (which are important for POP and $Mg^{2+}{}_A$ ion stabilization) is less than 1.6 Å. Similarly, RMSD measured for the products (UD1 and POP) and two Mg^{2+} ions is less than 1.6 Å during 5 ns NVT simulation. During 5 ns NVT simulation, $Mg^{2+}{}_A$ and $Mg^{2+}{}_B$ retained a stable hexa-coordination geometry, which is also seen in the crystal structure. $Mg^{2+}{}_A$ has one coordination interaction with Asp114, one with Asn239, two with water molecules and two with UD1. Similarly, the hexacoordinated geometry of $Mg^{2+}{}_B$ formed by its interactions with three water molecules, UD1 and POP remains stable. Stabilizing interactions of POP with the residues Gly17, Thr18, Arg19 and Lys26 provided by T1 region remain intact throughout the simulation. The interactions of POP with T1 region of the pocket include: (i) H-bond interactions made by P1 phosphate of POP with the backbone amide of Gly17 and the side chain of Lys26 and, (ii) H-bond interactions made by P2 phosphate with the side chains of Thr18 and Arg19.

The complete release of pyrophosphate into the solvent

In order to examine entire process of POP release from the active site into the solvent, we carried out US simulations, starting from the structure obtained from the last frame of NVT simulation. US simulations were carried out using d[PA-POP_{COM}] as the collective variable (CV). d[PA-POP_{COM}] is the distance between PA phosphorous of UD1 and the center of mass of P1, O_b and P2 of POP (Fig. S5a). P1 and P2 are two phosphorus atoms of POP, and O_b is the bridging oxygen between P1 and P2. Umbrella windows were placed for the distance d[PA-POP_{COM}], in the range of 5.4 Å to 21 Å. The restraint potential applied for each umbrella is listed in Table S3. In each umbrella window, simulations were run for 30 ns.

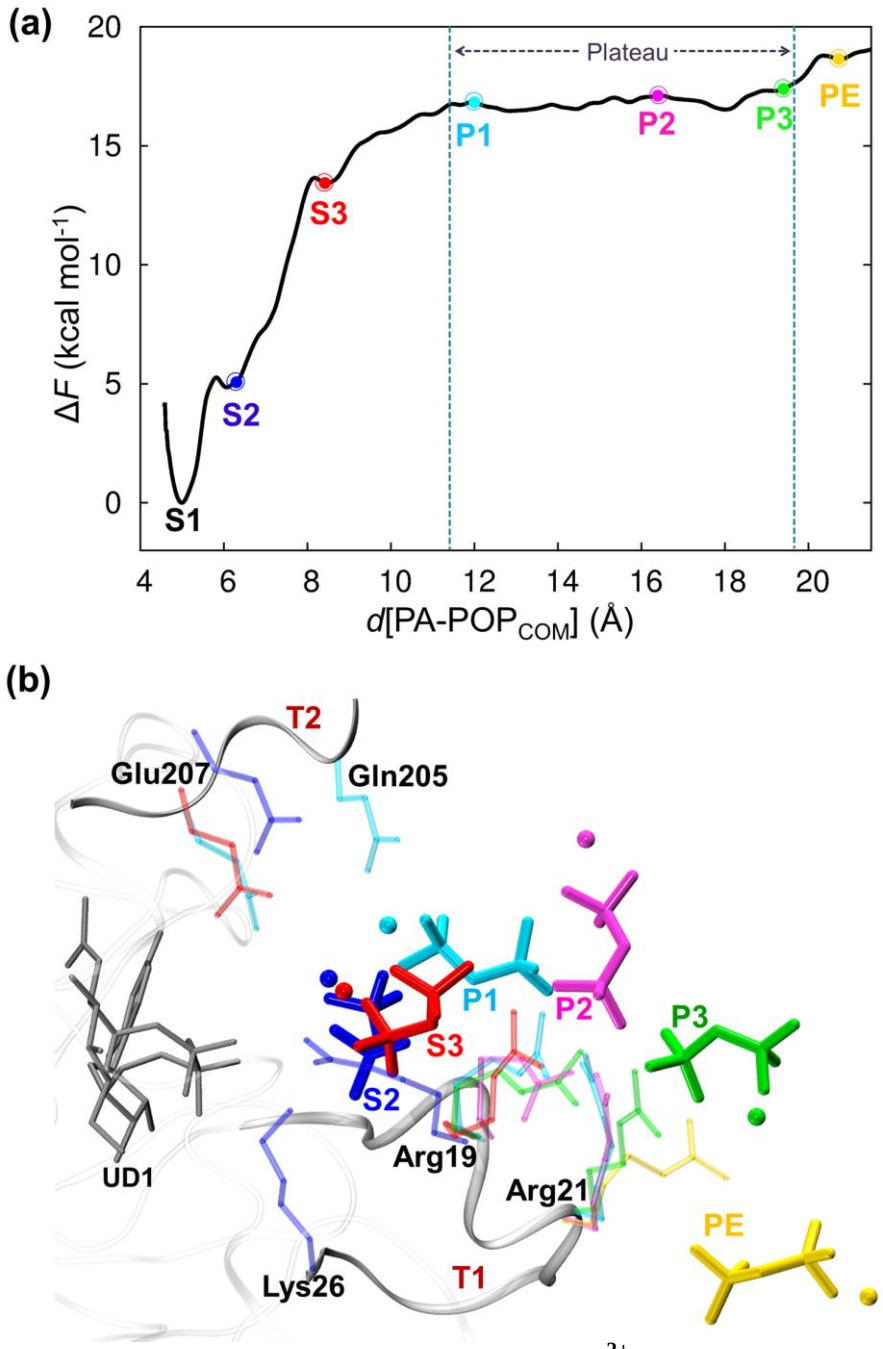

Figure 3. Free energy barrier and pathway for POP-Mg^{2+}_B release obtained from the US simulations. (a) Free energy profile for release of POP-Mg^{2+}_B from **S1** (the initial state) into the bulk solvent is shown. The intermediate states, **S2** and **S3**, three representative structures, **P1**, **P2** and **P3** (chosen arbitrarily) on the plateau, and the state **PE** where POP is released into the solvent are marked on the free energy profile. **(b)** POP, Mg^{2+}_B and the interacting pocket residues are shown for the states **S2** (blue), **S3** (red), **P1** (cyan), **P2** (magenta), **P3** (green) and **PE** (yellow). For each state, only the residues interacting with POP and Mg^{2+}_B are shown in the transparent sticks. The water molecules coordinating to Mg^{2+}_B are not shown for the purpose of clarity. T1 and T2 region are shown in ribbon form. Note the change in Arg19 side chain conformation as POP transitions beyond **S2**.

Free energy profile obtained from the US simulations shows that before POP is completely released in the bulk solvent, it passes through two intermediate states termed **S2** and **S3** (Fig. 3a). The initial state, termed **S1**, is the most stable and represents the state where UD1, POP and two Mg^{2+} ions are bound at the active site, following uridyltransfer reaction. Structures obtained from the umbrella corresponding to **S1**, highly resemble the snapshot GlmU[S1] in terms of the position occupied by POP and its interactions with T1 region (Fig. 4a, Table S4). $Mg^{2+}{}_B$ remains coordinated to POP in **S1** state. Glu207 from T2 stabilizes the water molecules coordinating $Mg^{2+}{}_B$. In **S1**, POP makes interactions with the side chains of Thr18, Arg19 and Lys21, and the backbone of Gly16 and Arg19. These interactions with T1 and T2 are also present in GlmU[S1]. Comparison of the interactions observed in **S1** and GlmU[S1] is provided in Table S4 (Supporting information; section 3.1).

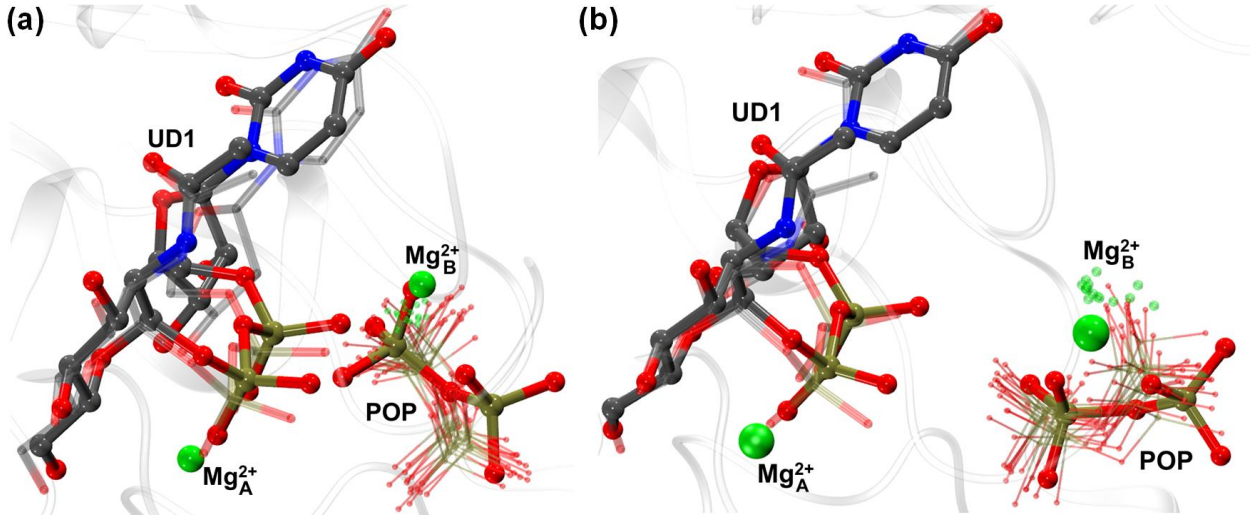

Figure 4. Comparison of S1 and S2 states with the structural snapshots. (a) Comparison of the **S1** state with GlmU[S1]. UD1, POP, $Mg^{2+}{}_A$ and $Mg^{2+}{}_B$ bound at the active site of GlmU[S1] are shown in thicker ball and stick representation, while those obtained from umbrella window corresponding to the **S1** state are shown as transparent ball and stick. **(b)** Comparison of the **S2** state with GlmU[S3]. Products and two Mg^{2+} ions from GlmU[S3] are shown in thicker ball and stick form, while those from US simulation are shown in transparent ball and stick form. POP and $Mg^{2+}{}_B$ are shown for the frames obtained from US simulations performed for 30 ns. The orientation of the active site differs from that of **A**, to highlight the overlap of POPs in **S2** and GlmU[S3].

From **S1**, POP proceeds to an intermediate state **S2**, crossing free energy barrier of 5 kcal mol^{-1}. Interestingly, the position occupied by POP in **S2** is similar to the position of BPOP observed in GlmU[S2] and GlmU[S3] snapshots (Fig. 4b). During the transition from **S1** to **S2**,

POP continues to retain its coordination interactions with Mg^{2+}_{B}, which aligns with the interactions it makes in the crystal structures GlmU[S2] and GlmU[S3] (Fig. 2, Supporting information; section 3.1). One of the water molecules coordinating Mg^{2+}_{B} is stabilized by Glu205 present in the T2 region of the exit pocket. These interaction of Glu205 is also observed in GlmU[S2] and GlmU[S3]. In **S2,** POP is stabilized by H-bond interactions with the backbone amides and side chains of Thr18 and Arg19 of T1 region (Supporting information; Fig. S4c). The same residues are observed to make stabilizing interactions with POP (in position B) in snapshots GlmU[S2] and GlmU[S3]. Unlike in GlmU[S2] and GlmU[S3], POP in **S2** retains its H-bond interaction with Lys26. Comparison of the interactions made by POP in **S2** and the snapshots GlmU[S2] and GlmU[S3] is provided in Table S4 (Supporting information; section 3.1).

For the reasons stated above, structural studies could not capture the movement of POP beyond position B i.e. beyond the state **S2**. On the other hand, US simulations illustrate POP movement beyond **S2** and show that the rate determining step is POP release beyond **S2**. The transition of POP from the state **S2** to **S3** requires crossing a free energy barrier of ~9 kcal mol^{-1} (Fig. 3a). This could be due to breaking and rearrangement of several H-bonds between POP and pocket residues during this transition. H-bond interactions of POP with Thr18 backbone amide and Lys26 side chain of T1 region break when it passes from **S2** to **S3** state. During this transition, Arg19 side chain flips from an inward facing conformation (Conf-A) to a conformation (Conf-B) facing the bulk solvent (Fig. 3 & Fig. 5). This change in conformation appears to trigger POP movement from **S2** to **S3** state. As a result, H-bond interactions of POP with Arg19 are rearranged. Specifically, the H-bonds between Arg19 and P1 phosphate (of POP) break, while those between Arg19 and P2 phosphate (of POP) form subsequently.

Following the state **S3**, POP passes through the states on a free energy plateau, before its complete release into the bulk solvent (Fig. 3). Three structures **P1**, **P2** and **P3** are chosen arbitrarily for representing the states on the free energy plateau as shown in Fig 4. On the plateau, POP retains its interactions with Arg19 side chain, while rest of its interactions with T1 and T2 regions break (Fig. 3). Notably, new H-bonds between POP and the side chain of Arg21 (of T1 region) set in simultaneously. Beyond the plateau, in state **PE** (fig. 4), interactions of POP with Arg19 break, while its interactions with Arg21 are retained. Thus, POP is passed on from one positively charged residue (Arg 19) to another (Arg 21) on the surface of T1 region (Fig. 3),

before it is completely released into the bulk solvent. Interestingly, the conformation of Arg19 highly resembling Conf-B has also been noted by Zhang et. al., in an apo GlmU structure (Fig. S5d) (Zhang et al., 2009).

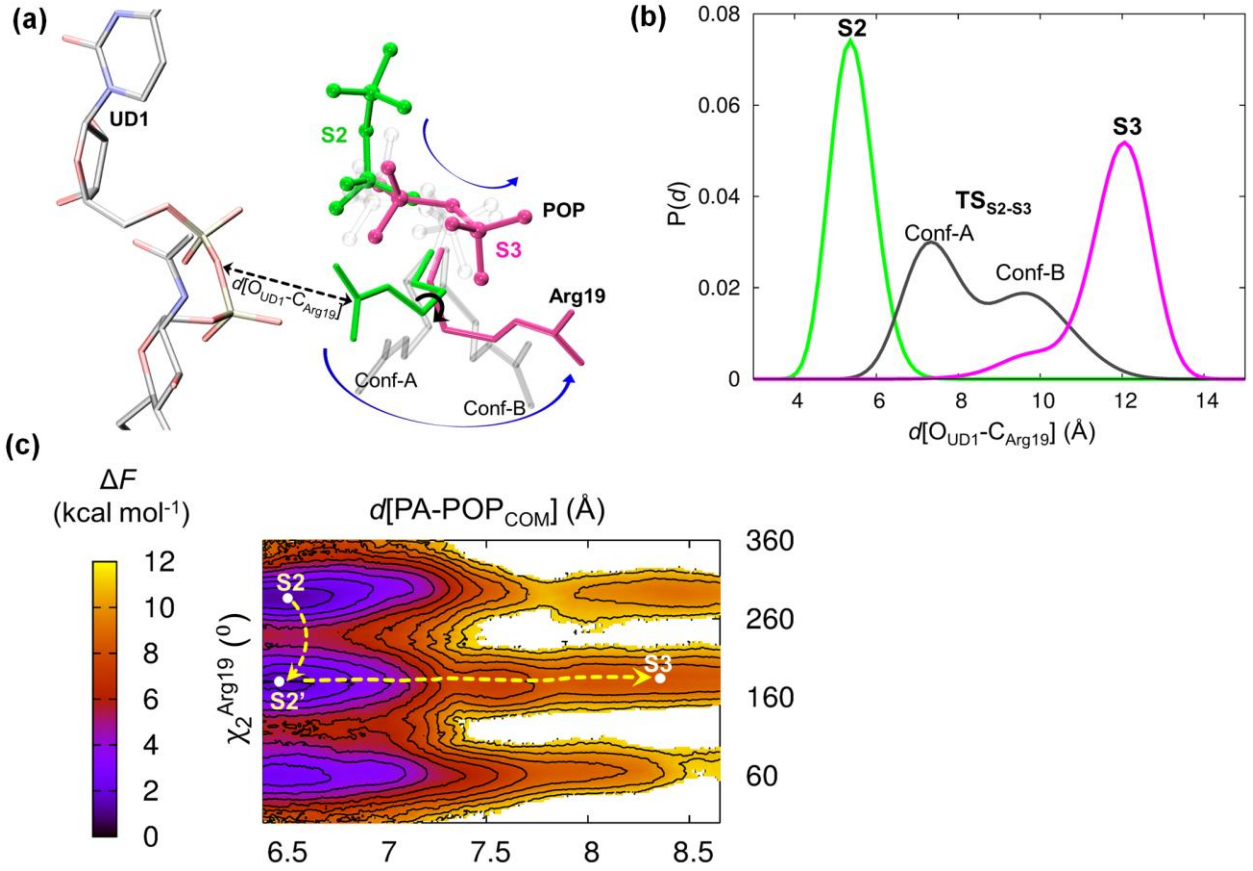

Figure 5. Rotation of Arg19 side chain during POP release from the S2 to S3 state. (a) Arg19 side chain and POP are shown for the **S2** (green color), **S3** (magenta color) and for the transition state (gray color) between **S2** and **S3** states. UD1 is shown in stick representation. **(b)** Probability distribution of, $d[O_{UD1}\text{-}C_{Arg19}]$, the distance between UD1 oxygen and side chain Cz carbon of Arg19 for the umbrella windows corresponding to the **S2** (green), **S3** (magenta) states and the transition state for **S2** to **S3** transition i.e. $\mathbf{TS_{S2\text{-}S3}}$ (black). This distance is labeled in **(a)**. For the $\mathbf{TS_{S2\text{-}S3}}$ umbrella window, two peaks are seen for $d[O_{UD1}\text{-}C_{Arg19}]$, representing Conf-A and Conf-B for Arg19 side chain. **(c)** Reconstructed free energy surface from TASS simulation for **S2** to **S3** transition. The free energy surface is projected as a function of two CVs, $d[PA\text{-}POP_{COM}]$ and χ_2^{Arg19} (i.e. TORSION[C_B:C_G:C_D:Ne]). χ_2^{Arg19} is defined by the rotation around CG-CD bond of Arg19 side chain (shown in **(a)** with black curved arrow). Contour lines are drawn at every 1 kcal mol^{-1}. The minimum energy path for **S2** to **S3** transition is shown by the dotted lines. **(d)** A model proposed for the mechanism of UTP entry into the active site, driven by the change in conformation of Arg19 from Conf-B to Conf-A. The atoms of only the triphosphate group of UTP are shown (ball and stick representation), while rest of the atoms of UTP are collectively represented as the large, transparent sphere connected to the triphosphate group. The color notations are the same as those used in **(a)**.

In US simulations, convergence of free energy profile can be slow if the auxiliary CVs such as H-bond interactions of POP with the pocket residues are not sampled properly. This could result in erroneous free energy estimates in US simulations. Besides, there is also a possibility of POP-Mg^{2+}_{B} complex dissociation during the process of POP release. In order to take into account all of these interactions of POP with pocket residues and Mg^{2+}_{B} ion, one needs to sample a large number of CVs along with d[PA-POP_{COM}]. Such extensive sampling would not be possible with US simulations. Thus, we employ TASS technique that allows sampling of a large number of CVs without requiring long simulations (Awasthi and Nair, 2017). As we found from our US simulations that there is major energy barrier (9 kcal mol^{-1}) during **S2** to **S3** transition, which requires conformational change of Arg19 side chain and rearrangement of several H-bonds between POP and pocket residues, we carried out TASS simulations for **S2** to **S3** transition. For this, d[PA-POP_{COM}] was sampled by umbrella bias, where the sampling window is from 6.1 to 9.0 Å (Supporting information; Table S3). Additionally, torsional angles of Arg19 side chain, H-bond interactions of POP with Arg19 and Lys26, and coordination interactions between POP and Mg^{2+}_{B} were sampled at a higher temperature (600 K) in each umbrella window (Supporting information; section 3.2, Table 2). Free energy profile obtained from TASS simulations, performed for 30 ns per umbrella window, provides the free energy barrier of 7 kcal mol^{-1} for **S2** to **S3** transition (Fig. 5c, Supporting information; Fig. S5c). The free energy surface, reconstructed as a function of d[PA-POP_{COM}] and Arg19 side chain dihedral angle, identifies the minimum energy pathway for the movement of POP-Mg^{2+}_{B} from **S2** to **S3**. The minimum energy path, denoted by the dotted lines on the free energy profile (Fig. 5c), shows that Arg19 side chain in the **S2** state rotates and leads to **S2'** state, which can facilitate the transition to **S3** state. The free energy landscape (Fig. 5c) also highlights that the S2 to S3 transition is possible with both – Conf-A and Conf-B conformations. However, the free energy barrier for this transition is lower by ~ 2 kcal mol^{-1} when Arg19 is in Conf-B. In the US simulations where the conformational changes of Arg19 were not sampled, we observed that Arg-19 largely occurs in Conf-A in the S2 state; this results in a higher free energy barrier (~ 2 kcal mol^{-1}) for S2 to S3 transition compared to that computed from the TASS simulations. Sampling of coordination interactions between POP and Mg^{2+}_{B} in TASS simulations confirms that POP-Mg^{2+}_{B} complex always remains intact. The free energy barrier obtained from US and

TASS simulations, for the complete release of POP from the active site pocket into the bulk solvent, is 18 kcal mol^{-1} (Supporting information; Fig. S5c). With such high energy barrier, product release appears to be a rate limiting factor in the catalytic cycle of the nucleotidyltransfer reaction of GlmU.

Previously, the movement of Mg^{2+} ion during product release was speculated in an SNT.(Schmidt et al., 2011) Metal ion mediated product release has also been suggested for glycosyltransferases, which share structural homology to SNTs (Hosfield et al., 2004; Lairson et al., 2008). A study on phosphoribosyltransferase enzymes has also elucidated that POP release occurs in complex with two Mg^{2+} ions. MD simulation studies carried out on RNA polymerases demonstrated that POP exits a pocket in complex with a Mg^{2+} ion (the one that is analogous to Mg^{2+}_{B} of SNT) (Da et al., 2012, 2013). In this study, we provide structural evidence and the mechanism for POP release in complex with Mg^{2+}_{B}.

Conservation of the POP release mechanism in SNTs.

POP-Mg^{2+}_B release along a pocket occurs via two intermediate states, which are stabilized by the residues present in T1 and T2 regions lining the exit pocket. T1 region, formed by the side chains of Arg19, Lys26 and the backbone amides of Gly17, Thr18 and Arg19, provide the positively charged surface for stabilization of POP in GlmU. These residues are conserved (Supporting information; Fig. S6) and form a signature motif L-X_2-G-X-G-T-R-M-X_4-P-K common to all SNTs (Mio et al., 1998). We identify that Arg19 also plays a crucial role in POP release by driving POP out of the pocket.

We have previously shown that the two-metal ion mechanism identified in GlmU would be operative in all SNTs (Jagtap et al., 2013). We divided SNTs into two major groups - Group-I and Group-II - based on the presence or absence of Mg^{2+}_A in SNTs (Jagtap et al., 2013). Group-II SNTs employ a single metal ion for catalysis, where the role of Mg^{2+}_A is replaced by a lysine residue. However, Mg^{2+}_B is invariably recruited for nucleotidyltransfer by both Group-I and Group-II SNTs (Jagtap et al., 2013). Mg^{2+}_B and the pocket residues, more importantly Arg19, are conserved across all SNTs (Fig. S6). Therefore, we propose that POP release in complex with Mg^{2+}_B would follow the same pathway and mechanism in all SNTs.

In DNA and RNA polymerases too, two Mg^{2+} ions (Mg^{2+}_A and Mg^{2+}_B) are utilized for the catalysis. Computational studies on POP release mechanism in RNA polymerase II and prokaryotic RNA polymerase suggest that POP exits as POP-Mg^{2+}_B complex (Da et al., 2012, 2013). In phosphoribosyltransferases also, POP release occurs in complex with two Mg^{2+} ions (Karmakar et al., 2016). This suggests that the POP release accompanied by Mg^{2+} ion(s) could be a common theme in a diverse class of enzymes that perform phosphoryl transfer reactions in the presence of Mg^{2+} ions.

Conclusions

We elucidate the process of POP release from the active site of GlmU – a nucleotidyltransferase enzyme, using structural and computational studies. In the product bound structure of GlmU, POP was observed to make coordination interactions with one of the catalytic Mg^{2+} ions (Mg^{2+}_B). The simulations presented here depict that POP exits the active site in complex with Mg^{2+}_B ion through a pocket. Release of POP-Mg^{2+} has been observed through computational studies in diverse enzymes catalyzing phosphoryltransfer reactions (Da et al., 2012, 2013;

Karmakar et al., 2016). This study provides a structural evidence for this phenomenon. The complete release of POP-Mg^{2+}_{B} complex in the bulk water occurs via two intermediate states. One of these intermediates is also captured in our crystallographic snapshots. Based on structural snapshots and the simulations, we identify the pocket residues stabilizing the intermediates. A conserved arginine (Arg19 in GlmU), which also lines the exit pocket, is identified to drive POP release from the pocket into the bulk water. POP release in SNTs appears to be the rate determining step in the catalytic cycle of the nucleotidyltransfer reaction. Further investigation of the rate of the chemical transformation *per se* should firmly establish this.

STAR Methods

KEY RESOURCES TABLE

Chemicals, Peptides, and Recombinant Proteins		
PEG8000	Hampton Research	HR2-535
HEPES	Sigma-Aldrich	7365-45-9
$MgCl_2$	Sigma-Aldrich	7786-30-3
$CoCl_2$	Sigma-Aldrich	7646-79-9
GlcNAc-1-P	Sigma-Aldrich	31281-59-1
UTP	Sigma-Aldrich	108321-53-5
Deposited Data		
GlmU[S2]	This paper, deposited at PDB	PDB: 4G3S
GlmU[S3]	This paper, deposited at PDB	PDB: 4G3P
Software and Algorithms		
XDS	http://xds.mpimf-heidelberg.mpg.de/	N/A
AutoRickshaw	http://www.embl-hamburg.de/Auto-Rickshaw/	N/A
ProDrug server	http://davapc1.bioch.dundee.ac.uk/cgi-bin/prodrg	N/A
Coot	https://www2.mrc-lmb.cam.ac.uk/personal/pemsley/coot/	N/A
PROCHECK	https://www.ebi.ac.uk/thornton-srv/software/PROCHECK/download.html	N/A
AMBER	http://ambermd.org/	N/A
R.E.D. package	http://upjv.q4md-forcefieldtools.org/RED/	N/A
VMD	http://www.ks.uiuc.edu/Development/Download/download.cgi?PackageName=VMD	N/A
PLUMED	http://www.plumed.org/get-it	N/A

Contact for reagent and resource sharing

Further information and requests for resources and reagents should be directed to and will be fulfilled by the Lead Contact, Balaji Prakash (balaji.prakash@cftri.res.in).

Method Details

Crystallization and structure determination

a) Crystallization

The wild type GlmU from *Mycobacterium tuberculosis* was purified and crystals of GlmU in apo (termed GlmU[Apo]) were obtained as described previously (Parikh et al., 2009). Three different snapshots of GlmU bound to UD1, POP and two Mg^{2+} ion - $GlmU^{Mtb}$[S2] and $GlmU^{Mtb}$[S3] were obtained by soaking GlmU[Apo] crystals in a soak solution at 4°C . The soak solution consists of 10% PEG8000, 100 mM HEPES (pH 7.5), 20 mM $MgCl_2$, 4 mM $CoCl_2$, 10 mM UTP and 10 mM GlcNAc-1-P. The ligand bound crystals were cryo-protected in a cryo solution consisting of 20% ethylene glycol, 15% PEG8000, 100 mM HEPES (pH 7.5), 20 mM $MgCl_2$ and 4 mM $CoCl_2$ prior to X-ray diffraction experiments and data collection.

b) Data collection and processing

X-ray diffraction data were collected using an in-house Rigaku MicoMax007HF X-ray source equipped with a copper rotating anode, Varimax optics, Mar345dtb image plate detector and Oxford cryosystem 700 series cryostream. XDS program package was used to index, integrate and scale the data. The crystals belong to H3 (146) space group. The solvent content of the crystals was ~58% with one protein molecule per asymmetric unit. The details of structure determination and refinement are provided in Table 1. The structure factors and atomic coordinates for GlmU[S2] and GlmU[S3] have been deposited in the Protein Data Bank (PDB) with accession codes 4G3S and 4G3P, respectively.

c) Structure determination and Refinement

The structures of product bound GlmU were determined by molecular replacement method using AutoRickshaw (Panjikar et al., 2005, 2009). The structure of GlmU[Apo] (PDB ID: 3dJ4) was used as the search model. The coordinates for ligands (UD1, POP and Mg^{2+}) were obtained from Protein Data bank (PDB). The library parameters for these ligands were generated using ProDrug server (van Aalten et al., 1996). The initial models were subjected to several rounds of manual building in Coot (Emsley et al., 2010). The crystallization conditions contained Mg^{2+} as well as Co^{2+} ions. As it is difficult to distinguish between the electron densities of Mg^{2+} ion and Co^{2+} ion, we resorted to utilize the anomalous signal of cobalt (at 1.54 Å wavelength). For this, the data processed without merging the Bijvoet pairs, i.e. with anomalous signal, was combined with the phases of the search model to locate the position of the Co^{2+} ion in the asymmetric unit. The initial structure was refined in the absence of ligands with Refmac5 using maximum likelihood target function employing rigid body refinement (Murshudov, G.N.; Skubak, P.; Lebedev, A.A.; Pannu, N.S.; Steiner, R.A.; Nicholls R.A.; Winn, M.D.; Long, F.; Vagin, 2011). This was followed by restrained refinement. After several cycles of refinement, ligands (UD1, POP and Mg^{2+}) were fitted into the electron density. The protein model with ligands was refined using refmac5. The quality of the final model was assessed using PROCHECK (Laskowski et al., 1993). Identification of water molecules (using 1σ cut-off in 2Fo-Fc maps) around the Mg^{2+} ions was carried out by ensuring that there is no unaccounted density in the vicinity. The final refinement statistics are listed in Table 1.

Molecular Dynamics (MD) Simulations

a) System setup and methods

The initial coordinates for the classical simulation were obtained from the crystal structure of GlmU determined in complex with both the products (UD1 and POP) and two Mg^{2+} ions (PDB ID: 4G87). In this structure, the products are retained at the active site of GlmU (Jagtap et al., 2013). GlmU is a bifunctional enzyme with uridyltransferase activity at the N-terminal domain and the acetyltransferase activity at its C-terminal domain.(Mengin-Lecreulx and van Heijenoort, 1994) Both the active sites are independent of each other.(Mengin-Lecreulx and van Heijenoort, 1994) Therefore, in our simulations, GlmU was truncated to include only the N-terminal uridyltransferase domain. The first three turns from the LβH structure of the C-terminal domain

were also included as they have been experimentally shown to be important for the Uridyltransfer reaction.(Parikh et al., 2009). The LβH holds an α-helix of the N-terminal domain in a stable conformation which provides Asn239 coordinated to Mg^{2+}_{A}. To ensure that the α-helix of the N-terminal domain remains in a stable conformation, the LβH was held in a stable conformation by harmonic constraints throughout the simulations. The enzyme was solvated with 14453 TIP3P water molecules within a periodic box of dimension 70×88×96 $Å^3$. The system was neutralized by adding 15 Na^+ counter ions. The whole protein was treated with parm99 version of the AMBER force field (Cheatham et al., 1999). Force field parameters for the ligands (UD1, POP and two Mg^{2+} ions) were derived from the GAFF force field (Wang et al., 2004) which is compatible with standard AMBER force field, as available in the AMBER suite of programs (Pearlman et al., 1995). Missing force field parameters for the ligands were not present in the GAFF force field, and were derived using Antechamber (Wang et al., 2006) tool available in AMBER package (parameters provided in Supporting information; section 2, Table S1). RESP charges were calculated for UD1, POP and two Mg^{2+} ions by the R.E.D. (Bayly et al., 1993; Dupradeau et al., 2010; Vanquelef et al., 2011) package. See below for details of the RESP charge calculation. Classical MD simulations were carried out using the AMBER suite of programs (Pearlman et al., 1995). A 12Å cutoff distance was used while computing the non-bonded interactions. The long range electrostatic interactions were computed using the particle mesh Ewald (PME) method (Darden et al., 1993). After the preliminary minimization of the water molecules and the subsequent minimization of the whole system, NPT simulations were carried out for 1 ns at 300 K using Langevin thermostat (Loncharich et al., 1992) and 1 atm using Berendsen barostat. This was followed by 5 ns NVT simulation at the equilibrium volume. The time step of 1 fs was used for integrating the equations of motion.

RESP charges: RESP charges (Table S2) of the ligands i.e. UD1, pyrophosphate and two magnesium ions, were obtained using the R.E.D. package (Bayly et al., 1993; Dupradeau et al., 2010; Vanquelef et al., 2011). The coordinates of the active site for the charge calculation were obtained from the crystal structure of GlmU[S1] (Fig. S4a), which included both the UD1, POP and two Mg^{2+} ions (Mg^{2+}_{A} and Mg^{2+}_{B}). Besides, two active site amino acids that make direct coordination interactions to Mg^{2+}_{A} (Asp114 and Asn239) and Lys26 which makes a hydrogen bond interaction to the POP oxygen were also included in their truncated forms with Asp114 replaced by acetate ion and, Lys26 replaced by methylamine and Asn132 by acetamide. The total

charge of the active site was restrained to $-2e$. The computed RESP charges are given in table S2. The partial charges on the magnesium ion A and B are ~1.57 and 1.27, respectively. These are much less than the formal charge of +2e, due to their coordination interactions with the negatively charged ligands (phosphate groups). This is in line with the RESP charge calculated for the magnesium ion in an Mg-POP complex reported earlier (Karmakar et al., 2016).

b) Umbrella sampling (US) simulations

US simulations were carried out using GROMACS program (Abraham et al., 2015) with PLUMED plugin (Bonomi et al., 2009). The CV used for US is d[PA-POP_{COM}] – the distance between PA phosphorous of UD1 and the center of mass of P1, O_b and P2 of POP (Supporting information; section 3). The umbrella windows were placed for d[PA-POP_{COM}] CV in the range of 5.4 Å to 21.0 Å. The details of restraint parameters used for each umbrella are provided in the supporting information, section 3 (Table S3). The starting structure for the first window set at 5.4 Å was obtained from the NVT simulation run for 5 ns (described above). For rest of the umbrellas, the starting structure was obtained from adjacent umbrella equilibrated for ~ 1 ns. In each umbrella, NVT simulation was performed for 30 ns.

c) Temperature accelerated sliced sampling (TASS) simulations

TASS has been recently developed in our group which combines the techniques of US, metadynamics and temperature accelerated sampling for enhanced sampling of a large number of CVs (Awasthi and Nair, 2017). In the present study, we have used TASS method without adding any external bias potential i.e. only US and temperature accelerated sampling were combined. The parameters and starting structures used for each umbrella window remain the same as described above in US simulations. Additionally, orthogonal CVs (listed in Table 2) were sampled at 600 K temperature in each umbrella. For this, each CV was linked to an auxiliary variable using a mass μ_α of 100 a.m.u and k_α of 2.5 x 10^3 kcal mol^{-1}. Auxiliary variables associated with each CV were sampled at 600 K, using Langevin thermostat. Simulations were performed for 30 ns, in each umbrella.

Acknowledgements

US and TASS simulations were performed using the High Performance Computing (HPC) facility at IIT Kanpur. We thank Dr. Vinay Nandicoori, NII, New Delhi, for fruitful collaborations on GlmU. B.P. thanks CSIR-CFTRI, Mysore for continous support. The experimental work was supported by a grant (year 2009) from Department of Biotechnology, India. We also thank Department of Biotechnology, India, for the current grant (BT/PR12233/BRB/10/1349/2014). N.V. thanks IIT Kanpur for the PhD scholarship.

Author Contributions

N.V. performed MD simulations and collected X-ray crystallographic data. P.K.A.J. processed and analyzed the X-ray crystallographic data. S.K.V. set up the crystallization experiments and collected X-ray crystallographic data. R.T. and S.A. helped in the simulation studies. B.P. directed the experimental studies. N.N.N. directed the simulation studies. B.P., P.K.A.J., N.V. and N.N.N. wrote the manuscript.

Declaration of Interests

The authors declare no competing interests.

References

van Aalten, D.M.F., Bywater, R., Findlay, J.B.C., Hendlich, M., Hooft, R.W.W., and Vriend, G. (1996). PRODRG, a program for generating molecular topologies and unique molecular descriptors from coordinates of small molecules. J. Comput. Aided. Mol. Des. *10*, 255–262.

Abraham, M.J., Murtola, T., Schulz, R., Pall, S., Smith, J.C., Hess, B., and Lindah, E. (2015). Gromacs: High performance molecular simulations through multi-level parallelism from laptops to supercomputers. SoftwareX *1–2*, 19–25.

Awasthi, S., and Nair, N.N. (2017). Exploring high dimensional free energy landscapes: Temperature accelerated sliced sampling. J. Chem. Phys. *146*, 094108–094116.

Barreteau, H., Kovac, A., Boniface, A., Sova, M., Gobec, S., and Blanot, D. (2008). Cytoplasmic steps of peptidoglycan biosynthesis. FEMS Microbiol. Rev. *32*, 168–207.

Bayly, C.I., Cieplak, P., Cornell, W., and Kollman, P.A. (1993). A well-behaved electrostatic potential based method using charge restraints for deriving atomic charges: the RESP model. J. Phys. Chem. *97*, 10269–10280.

Bonomi, M., Branduardi, D., Bussi, G., Camilloni, C., Provasi, D., Raiteri, P., Donadio, D., Marinelli, F., Pietrucci, F., Broglia, R.A., et al. (2009). PLUMED: A portable plugin for free-energy calculations with molecular dynamics. Comput. Phys. Commun. *180*, 1961–1972.

Chang, H.Y., Lee, J.H., Deng, W.L., Fu, T.F., and Peng, H.L. (1996). Virulence and outer membrane properties of a galU mutant of Klebsiella pneumoniae CG43. Microb Pathog *20*, 255–261.

Cheatham, T.E., Cieplak, P., and Kollman, P.A. (1999). A Modified Version of the Cornell *et al.* Force Field with Improved Sugar Pucker Phases and Helical Repeat. J. Biomol. Struct. Dyn. *16*, 845–862.

Da, L.T., Wang, D., and Huang, X. (2012). Dynamics of pyrophosphate ion release and its

coupled trigger loop motion from closed to open state in RNA polymerase II. J. Am. Chem. Soc. *134*, 2399–2406.
Da, L.T., Pardo Avila, F., Wang, D., and Huang, X. (2013). A Two-State Model for the Dynamics of the Pyrophosphate Ion Release in Bacterial RNA Polymerase. PLoS Comput. Biol. *9*, e1003020.
Darden, T., York, D., and Pedersen, L. (1993). Particle mesh Ewald: An $N \cdot \log(N)$ method for Ewald sums in large systems. J. Chem. Phys. *98*, 10089–10092.
Dupradeau, F.-Y., Pigache, A., Zaffran, T., Savineau, C., Lelong, R., Grivel, N., Lelong, D., Rosanski, W., and Cieplak, P. (2010). The R.E.D. tools: advances in RESP and ESP charge derivation and force field library building. Phys. Chem. Chem. Phys. *12*, 7821–7839.
Emsley, P., Lohkamp, B., Scott, W.G., and Cowtan, K. (2010). Features and development of Coot. Acta Crystallogr. Sect. D Biol. Crystallogr. *66*, 486–501.
Frey, P.A. (1996). The Leloir pathway: a mechanistic imperative for three enzymes to change the stereochemical configuration of a single carbon in galactose. FASEB J. *10*, 461–470.
Hosfield, D.J., Zhang, Y., Dougan, D.R., Broun, A., Tari, L.W., Swanson, R. V., and Finn, J. (2004). Structural Basis for Bisphosphonate-mediated Inhibition of Isoprenoid Biosynthesis. J. Biol. Chem. *279*, 8526–8529.
Jagtap, P.K.A., Verma, S.K., Vithani, N., Bais, V.S., and Prakash, B. (2013). Crystal structures identify an atypical two-metal-ion mechanism for uridyltransfer in GlmU: Its significance to sugar nucleotidyl transferases. J. Mol. Biol. *425*, 1745–1759.
Karmakar, T., Roy, S., Balaram, H., Prakash, M.K., and Balasubramanian, S. (2016). Product Release Pathways in Human and Plasmodium falciparum Phosphoribosyltransferase. J. Chem. Inf. Model. *56*, 1528–1538.
Karmakar, T., Roy, S., Balaram, H., and Balasubramanian, S. (2016). Structural and dynamical correlations in PfHGXPRT oligomers: A molecular dynamics simulation study. J. Biomol. Struct. Dyn. *34*, 1590–1605.
Kästner, J. (2011). Umbrella sampling. Wiley Interdiscip. Rev. Comput. Mol. Sci. *1*, 932–942.
Lairson, L.L., Henrissat, B., Davies, G.J., and Withers, S.G. (2008). Glycosyltransferases: Structures, Functions, and Mechanisms. Annu. Rev. Biochem. *77*, 521–555.
Laskowski, R.A., MacArthur, M.W., Moss, D.S., and Thornton, J.M. (1993). PROCHECK: a program to check the stereochemical quality of protein structures. J. Appl. Crystallogr. *26*, 283–291.
Lassila, J.K., Zalatan, J.G., and Herschlag, D. (2011). Biological Phosphoryl-Transfer Reactions: Understanding Mechanism and Catalysis. Annu. Rev. Biochem. *80*, 669–702.
Loncharich, R.J., Brooks, B.R., and Pastor, R.W. (1992). Langevin dynamics of peptides: The frictional dependence of isomerization rates of N-acetylalanyl-N′-methylamide. Biopolymers *32*, 523–535.
McNeil, M., Daffe, M., and Brennan, P.J. (1990). Evidence for the nature of the link between the arabinogalactan and peptidoglycan of mycobacterial cell walls. J. Biol. Chem. *265*, 18200–18206.
Mengin-Lecreulx, D., and van Heijenoort, J. (1994). Copurification of glucosamine-1-phosphate acetyltransferase and N-acetylglucosamine-1-phosphate uridyltransferase activities of Escherichia-coli - characterization of the GlmU gene-product as a bifunctional enzyme catalyzing 2 subsequent steps in the path. J. Bacteriol. *176*, 5788–5795.
Mengin-Lecreulx, D., Flouret, B., and Van Heijenoort, J. (1982). Cytoplasmic steps of peptidoglycan synthesis in Escherichia coli. J. Bacteriol. *151*, 1109–1117.

Mio, T., Yabe, T., Arisawa, M., and Yamada-Okabe, H. (1998). The eukaryotic UDP-N-acetylglucosamine pyrophosphorylases: Gene cloning, protein expression, and catalytic mechanism. J. Biol. Chem. *273*, 14392–14397.
Murshudov, G.N.; Skubak, P.; Lebedev, A.A.; Pannu, N.S.; Steiner, R.A.; Nicholls R.A.; Winn, M.D.; Long, F.; Vagin, A.A. (2011). REFMAC5 for the refinement of molecular crystal structures. Acta Crystallogr D Biol Crystallogr *67*, 355–367.
Panjikar, S., Parthasarathy, V., Lamzin, V.S., Weiss, M.S., and Tucker, P.A. (2005). Auto-Rickshaw: An automated crystal structure determination platform as an efficient tool for the validation of an X-ray diffraction experiment. Acta Crystallogr. Sect. D Biol. Crystallogr. *61*, 449–457.
Panjikar, S., Parthasarathy, V., Lamzin, V.S., Weiss, M.S., and Tucker, P.A. (2009). On the combination of molecular replacement and single-wavelength anomalous diffraction phasing for automated structure determination. Acta Crystallogr. Sect. D Biol. Crystallogr. *65*, 1089–1097.
Parikh, A., Verma, S.K., Khan, S., Prakash, B., and Nandicoori, V.K. (2009). PknB-Mediated Phosphorylation of a Novel Substrate, N-Acetylglucosamine-1-Phosphate Uridyltransferase, Modulates Its Acetyltransferase Activity. J. Mol. Biol. *386*, 451–464.
Pearlman, D.A., Case, D.A., Caldwell, J.W., Ross, W.S., Cheatham, T.E., DeBolt, S., Ferguson, D., Seibel, G., and Kollman, P. (1995). AMBER, a package of computer programs for applying molecular mechanics, normal mode analysis, molecular dynamics and free energy calculations to simulate the structural and energetic properties of molecules. Comput. Phys. Commun. *91*, 1–41.
Schmidt, H., Mesters, J.R., Wu, J., Woodard, R.W., Hilgenfeld, R., and Mamat, U. (2011). Evidence for a two-metal-ion mechanism in the cytidyltransferase KdsB, an enzyme involved in lipopolysaccharide biosynthesis. PLoS One *6*, e23231.
Sosunov, V., Sosunova, E., Mustaev, A., Bass, I., Nikiforov, V., and Goldfarb, A. (2003). Unified two-metal mechanism of RNA synthesis and degradation by RNA polymerase. EMBO J. *22*, 2234–2244.
Steitz, T. a, and Steitz, J. a (1993). A general two-metal-ion mechanism for catalytic RNA. Proc. Natl. Acad. Sci. U. S. A. *90*, 6498–6502.
Torrie, G.M., and Valleau, J.P. (1974). Monte Carlo free energy estimates using non-Boltzmann sampling: Application to the sub-critical Lennard-Jones fluid. Chem. Phys. Lett. *28*, 578–581.
Vanquelef, E., Simon, S., Marquant, G., Garcia, E., Klimerak, G., Delepine, J.C., Cieplak, P., and Dupradeau, F.Y. (2011). R.E.D. Server: A web service for deriving RESP and ESP charges and building force field libraries for new molecules and molecular fragments. Nucleic Acids Res. *39*, W511-7.
Wang, J., Wang, W., Kollman, P.A., and Case, D.A. (2006). Automatic atom type and bond type perception in molecular mechanical calculations. J. Mol. Graph. Model. *25*, 247–260.
Wang, J.M., Wolf, R.M., Caldwell, J.W., Kollman, P. a, and Case, D. a (2004). Development and testing of a general amber force field. J. Comput. Chem. *25*, 1157–1174.
Zhang, Z., Bulloch, E.M.M., Bunker, R.D., Baker, E.N., and Squire, C.J. (2009). Structure and function of GlmU from Mycobacterium tuberculosis. Acta Crystallogr. Sect. D Biol. Crystallogr. *65*, 275–283.

Tables

Table 1. X-ray Diffraction Data - Data collection and refinement statistics

	GlmU[S2]	GlmU[S3]
Data collection		
Space group	H 3	H 3
Cell dimensions		
a, *b*, *c* (Å)	76.58,76.58,276.97	77.47,77.47,277.5
α, β, γ (°)	90,90,120	90,90,120
Resolution (Å)	2.04(2.09)	2.47(2.53)
R_{merge}(%)	7.2 (65.6)	11.4(57.3)
$I / \sigma I$	22.35(3.24)	16.4(3.45)
Completeness (%)	99.2(94.1)	99.3(92.8)
Redundancy	6.99(6.4)	6.31(5.76)
Refinement		
Resolution range (Å)	19.9-2.04	19.9-2.46
No. reflections	38392	21135
R_{work} / R_{free}	0.18/0.23	0.18/0.24
No. atoms		
Protein	3374	3374
Ligand/ion	81	52
Water	372	191
B-factors		
Protein	29.90	24.48
Ligand/ion	30.06	18.29
Water	40.20	27.47
RMSD		
Bond lengths (Å)	0.028	0.022
Bond angles (°)	2.18	2.01

*Numbers in paranthesis correspond to the last resolution shell.

Table 2. Orthogonal CVs sampled at 600 K temperature in TASS simulations. Here, O_{GroupA}: O1, O2, O3, O4, O5, O6; O_{GroupB}: O1, O2, O3; O_{GroupC}: O4, O5, O6

CV2	CN[Mg^{2+}_B:O_{GroupA}]	CV7	CN[$ArgNh_2$:O_{GroupC}]
CV3	CN[LysNz:O_{GroupA}]	CV8	TORSION[C_A:C_B:C_G:C_D]
CV4	CN[ArgNe:O_{GroupB}]	CV9	TORSION[C_B: C_G:C_D:Ne]
CV5	CN[ArgNe:O_{GroupC}]	CV10	TORSION[C_G:C_D:Ne:C_Z]
CV6	CN[$ArgNh_2$:O_{GroupB}]		